

Supporting Information

**In-situ Coupling of Multidimensional MOFs for
Heterogeneous Metal Oxide Architectures:
Toward Sensitive Chemiresistor**

Ji-Soo Jang,^{†,‡} Won-Tae Koo,^{†,‡} Dong-Ha Kim,^{†,‡} and Il-Doo Kim^{†,‡,}*

[†]Department of Materials Science and Engineering, Korea Advanced Institute of Science and Technology, 291 Daehak-ro, Yuseong-gu, Daejeon 305-701, Republic of Korea

[‡]Advanced Nanosensor Research Center, KI Nanocentury, KAIST, 291 Daehak-ro, Yuseong-gu Daejeon 34141, Republic of Korea

*E-mail: idkim@kaist.ac.kr

Table of Contents

- S1.** Additional TEM analysis and EDS mapping images
 - S2.** XRD analysis
 - S3.** Schematic illustration of fabrication process of ZIF-67 NRs
 - S4.** XRD analysis of various double- Co_3O_4 rods@ZnO sheets
 - S5.** SEM images of double- Co_3O_4 rods@ZnO sheets depending on the calcination temperature
 - S6.** SEM image of polyhedron ZIF-67 particles
 - S7.** SEM image of Zn based ZIF-L
 - S8.** SEM and TEM images of collapsed Co_3O_4 rods loaded ZnO sheet
 - S9.** EDS mapping images of calcined HMOFs
 - S10.** XPS spectra of heterogeneous Co_3O_4 rods@ZnO sheet
 - S11.** Temperature dependent acetone response
 - S12.** Extrapolation of the double- Co_3O_4 rods@ZnO sheet's detection limit
 - S13.** Resistance variation of Co_3O_4 rods, ZnO sheet, single- Co_3O_4 rods@ZnO sheet, double- Co_3O_4 rods@ZnO sheet, and triple- Co_3O_4 rods@ZnO sheet
 - S14.** XPS spectra of oxygen
 - S15.** N_2 adsorption/desorption isotherms
 - S16.** Schematic image of sensing measurement system
-
- Table S1.** The pH values of 4 ZIFs solutions
 - Table S2.** Grain sizes of samples based on the (100), (002), and (101) peaks
 - Table S3** ICP results
 - Table S4.** The surface area under XPS spectra of O 1s
 - Table S5** Recent publications on MOF derived SMOs based chemiresistive acetone sensors
 - Table S4.** Recent publications on MOF based chemiresistive sensors

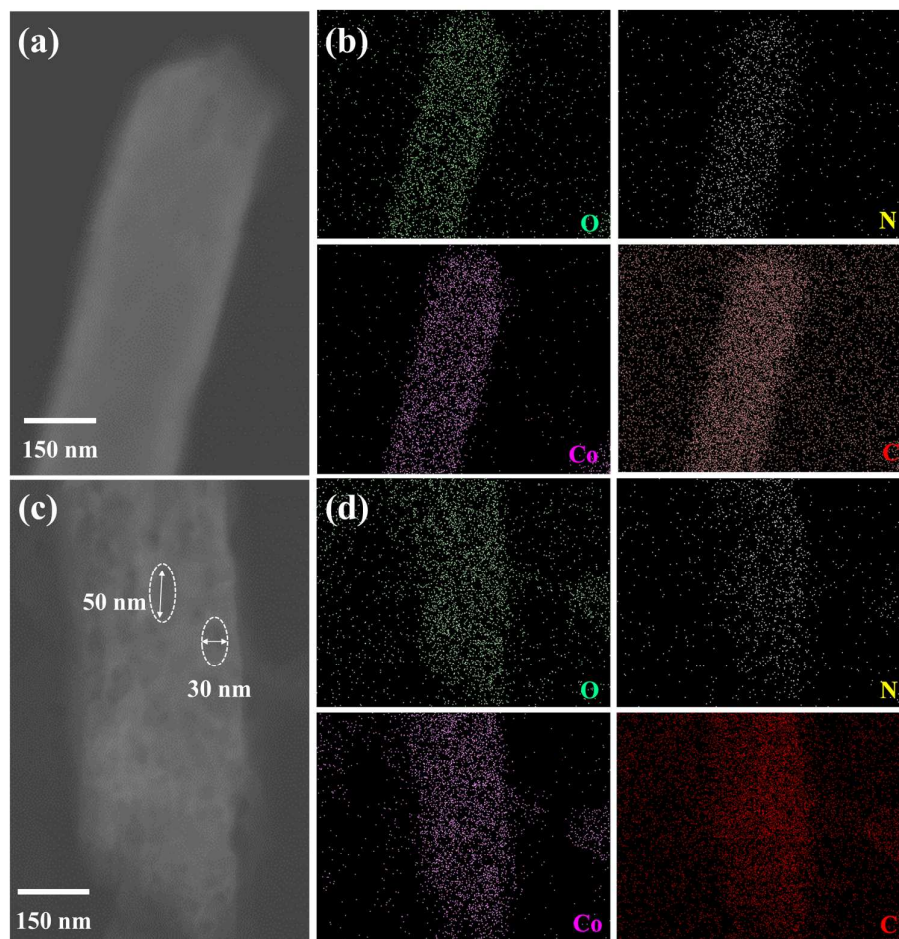


Figure S1. STEM images of (a) ZIF-67 rods and (c) ZIF-67 belts, EDS mapping images of (b) ZIF-67 rods and (d) ZIF-67 belts with Co, O, C, and N elements.

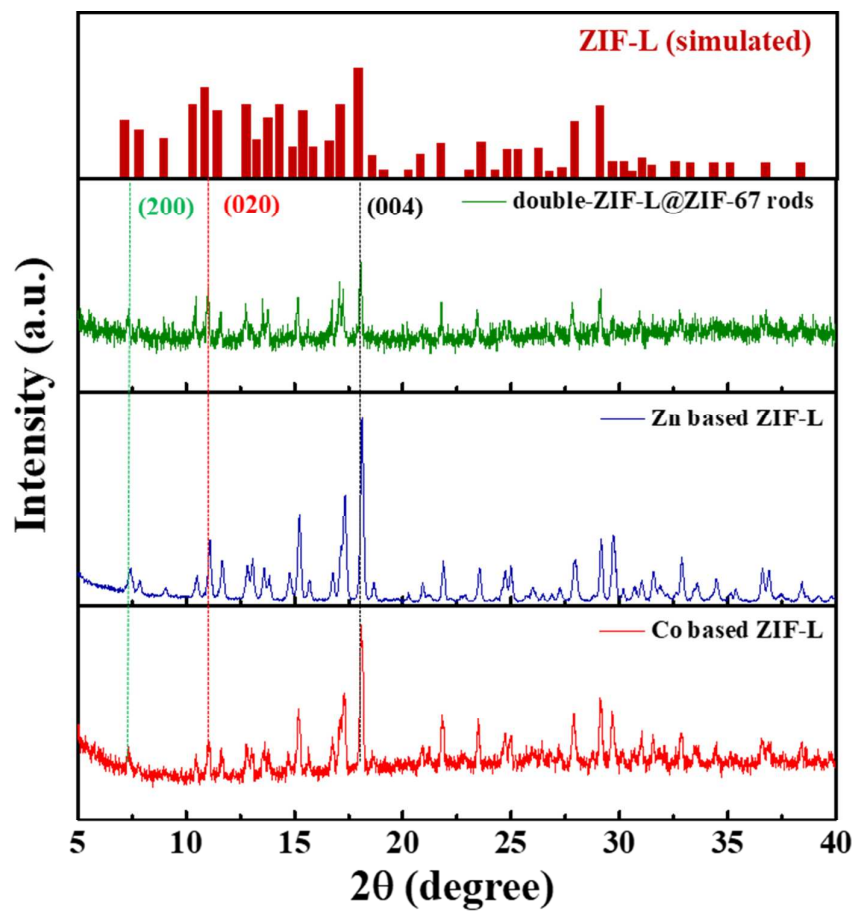


Figure S2. XRD analysis of Co based ZIF-L, Zn based ZIF-L, and double-ZIF-L@ZIF-67 rods.

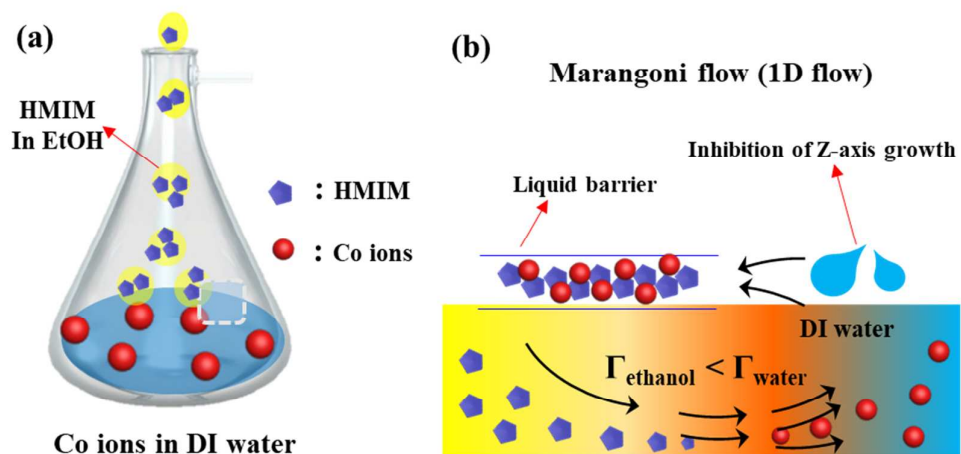


Figure S3. (a) Schematic image showing mixing process of HMIM dissolved solution and Co ions dissolved solution, (b) schematic illustration of Marangoni flow between HMIM-EtOH and Co ions-DI water solutions.

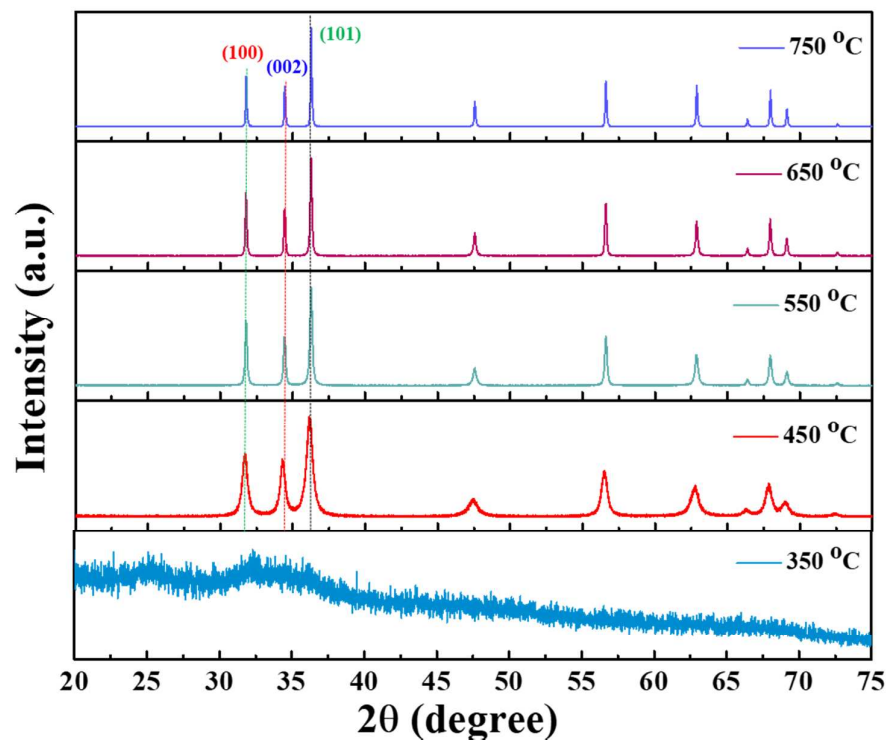


Figure S4. XRD analysis of various double-Co₃O₄ rods@ZnO sheets (e.g. 350 double-Co₃O₄ rods@ZnO sheet, 450 double-Co₃O₄ rods@ZnO sheet, 550 double-Co₃O₄ rods@ZnO sheet, 650 double-Co₃O₄ rods@ZnO sheet, and 750 double-Co₃O₄ rods@ZnO sheet)

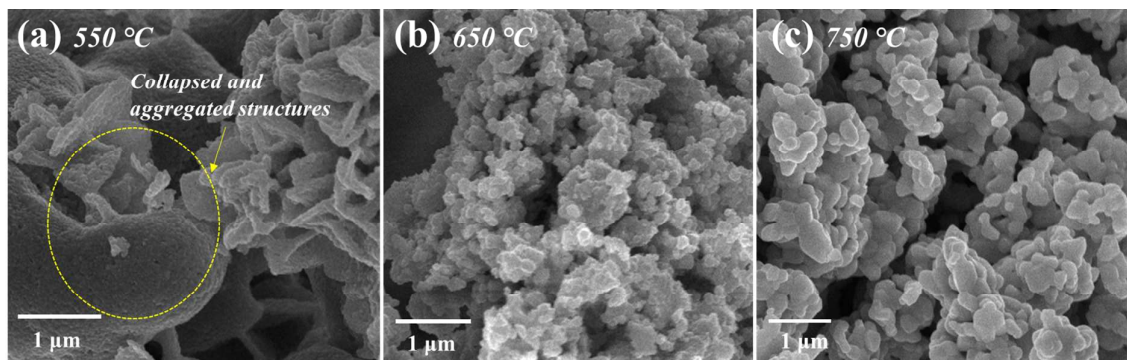


Figure S5. SEM image of (a) 550 double-Co₃O₄ rods@ZnO sheets, (b) 650 double-Co₃O₄ rods@ZnO sheets, and (c) 750 double-Co₃O₄ rods@ZnO sheets.

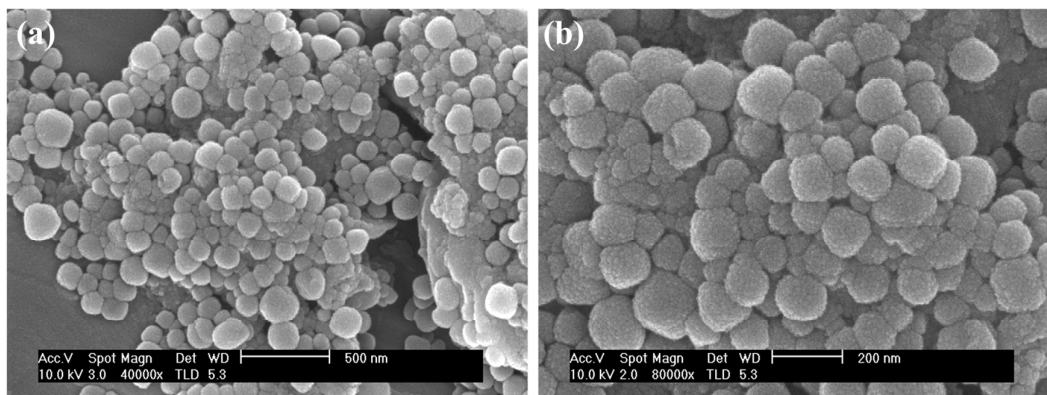


Figure S6. (a) SEM image of polyhedron ZIF-67 particles produced by using mixed solvent of DI water and EtOH. (b) Magnified SEM image of polyhedron ZIF-67.

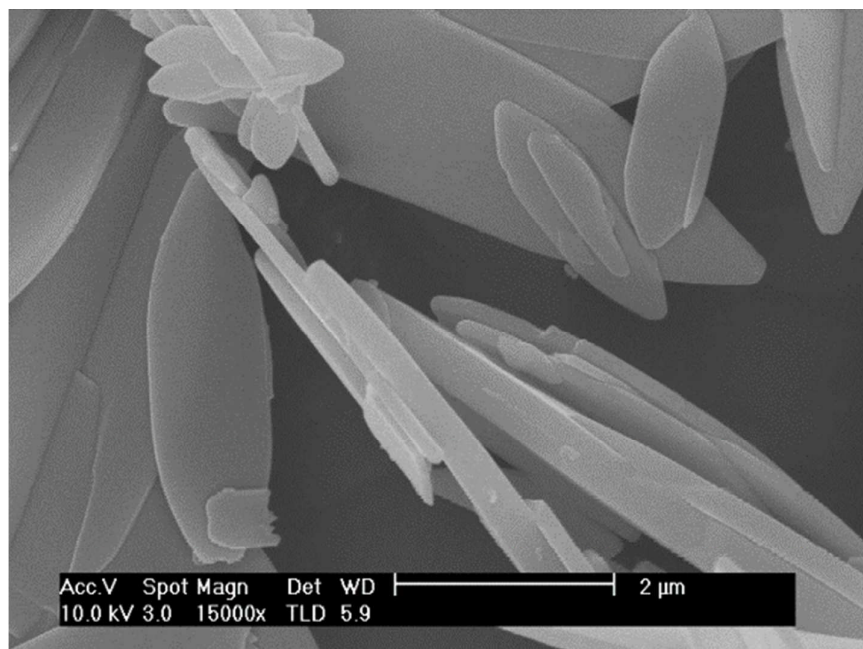


Figure S7. SEM image of Zn based ZIF-L structures.

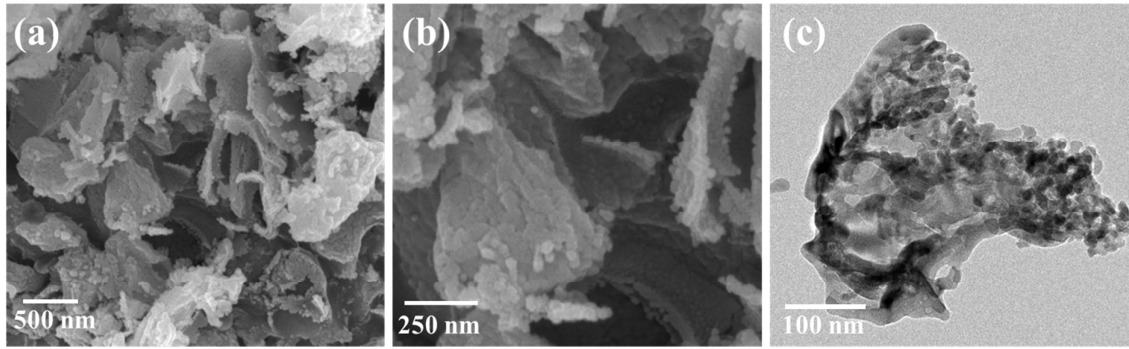


Figure S8. SEM images of (a, b) collapsed Co_3O_4 rods loaded ZnO sheet, and (c) TEM image of collapsed Co_3O_4 rods loaded ZnO sheet.

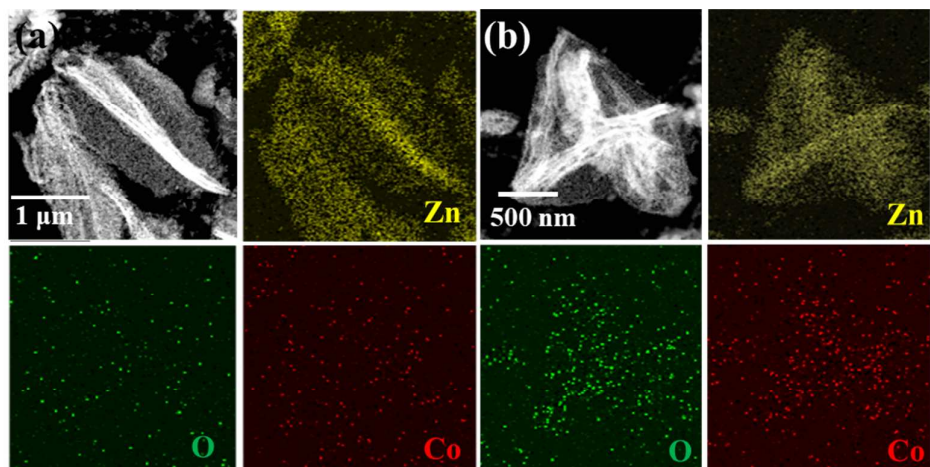


Figure S9. EDS mapping images of (a) single-Co₃O₄ rods@ZnO sheet, and (b) double-Co₃O₄ rods@ZnO sheet.

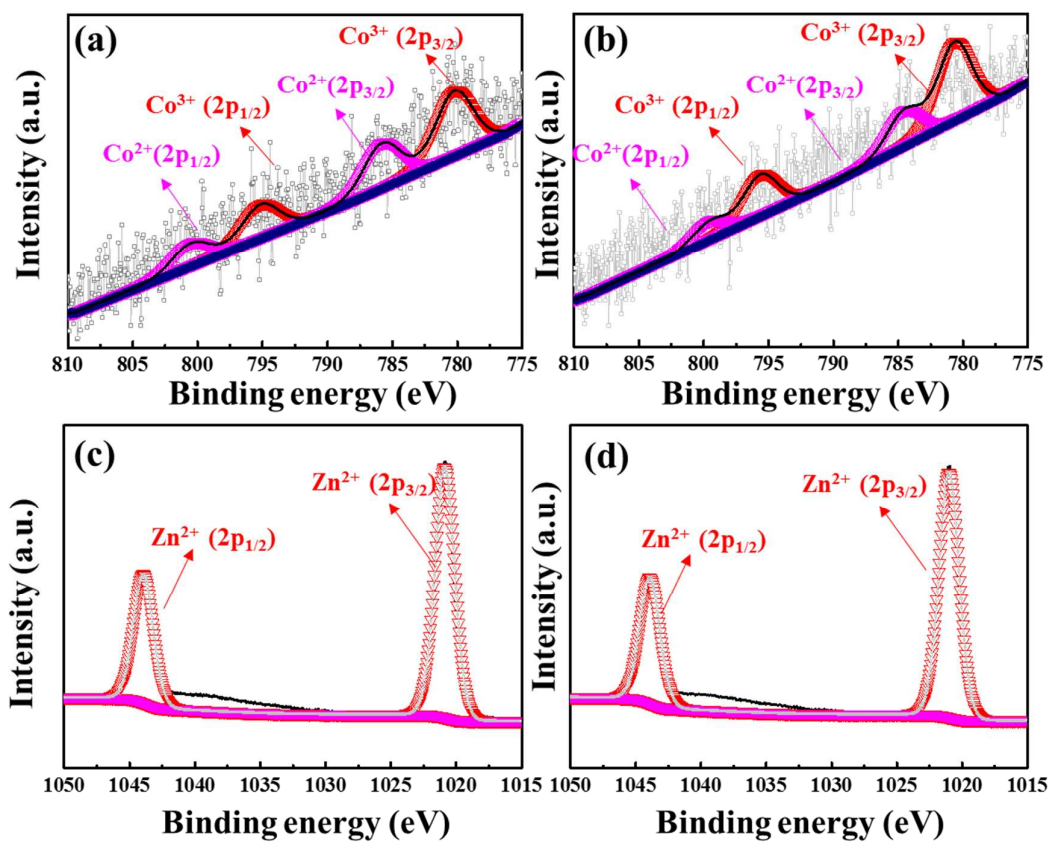


Figure S10. XPS spectra of single-Co₃O₄ rods@ZnO sheet: (a) Co 2p and (c) Zn 2p, and XPS spectra of double-Co₃O₄ rods@ZnO sheet: (b) Co 2p and (d) Zn 2p.

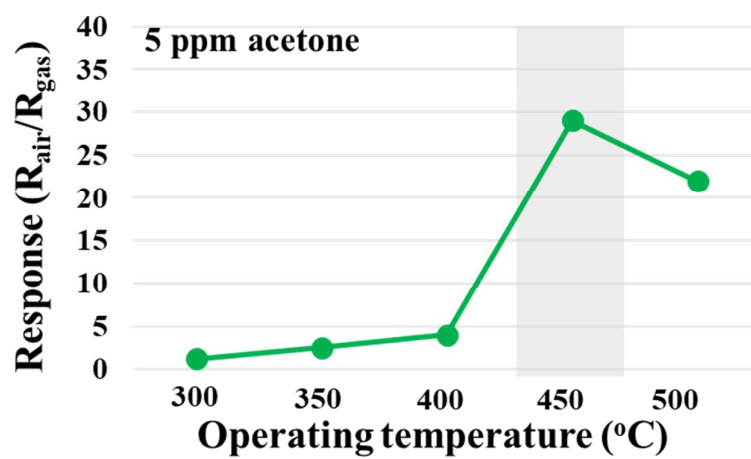


Figure S11. Acetone sensing response of double- Co_3O_4 rods@ZnO sheet at various sensing temperatures.

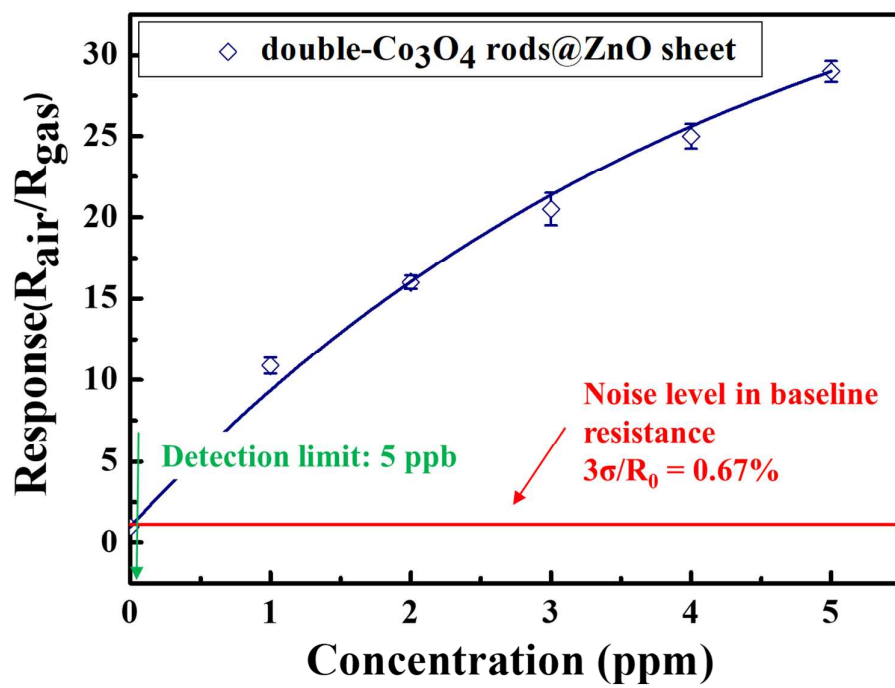


Figure S12. Extrapolation of the double- Co_3O_4 rods@ZnO sheet's detection limit toward acetone gas at 450 □

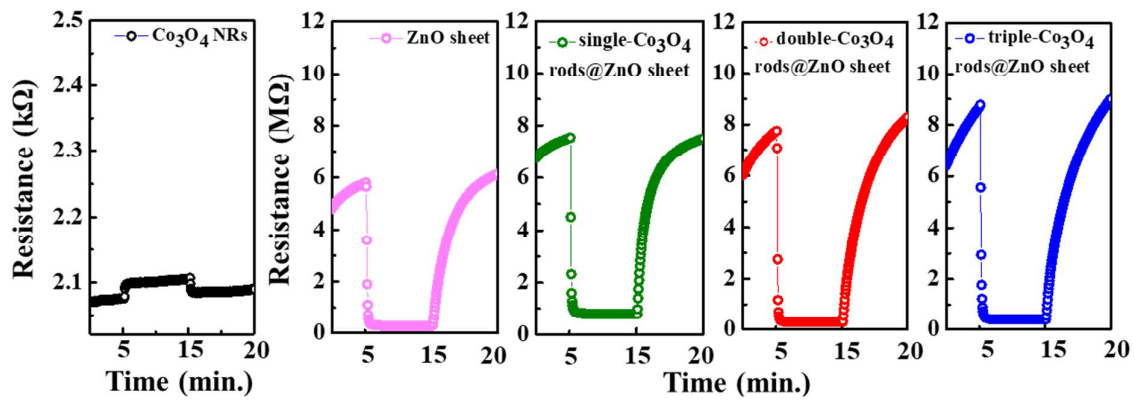


Figure S13. Resistance variation of Co₃O₄ rods, ZnO sheet, single-Co₃O₄ rods@ZnO sheet, double-Co₃O₄ rods@ZnO sheet, and triple-Co₃O₄ rods@ZnO sheet upon exposure to 5 ppm of acetone at 450 °C.

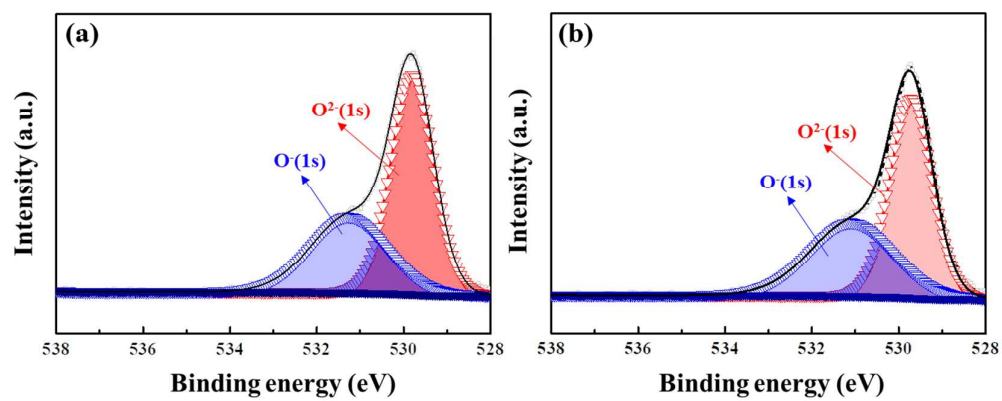


Figure S14. XPS spectra of oxygen in (a) single-Co₃O₄ rods@ZnO sheet, and (b) triple-Co₃O₄ rods@ZnO sheet.

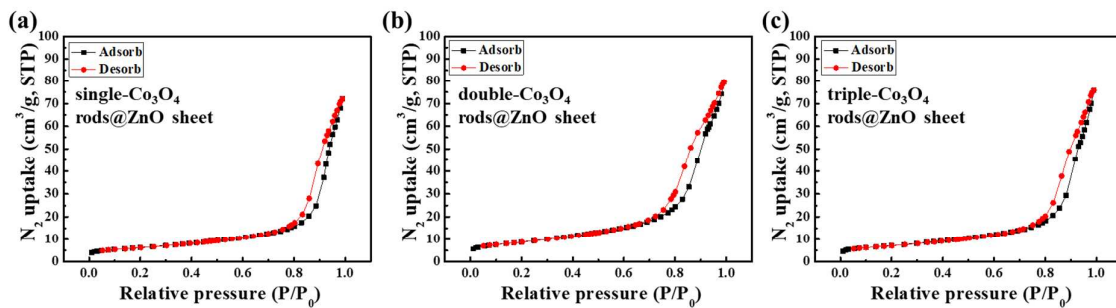


Figure S15. N₂ adsorption/desorption isotherms of (a) single-Co₃O₄ rods@ZnO sheet, (b) double-Co₃O₄ rods@ZnO sheet, and (c) triple-Co₃O₄ rods@ZnO sheet.

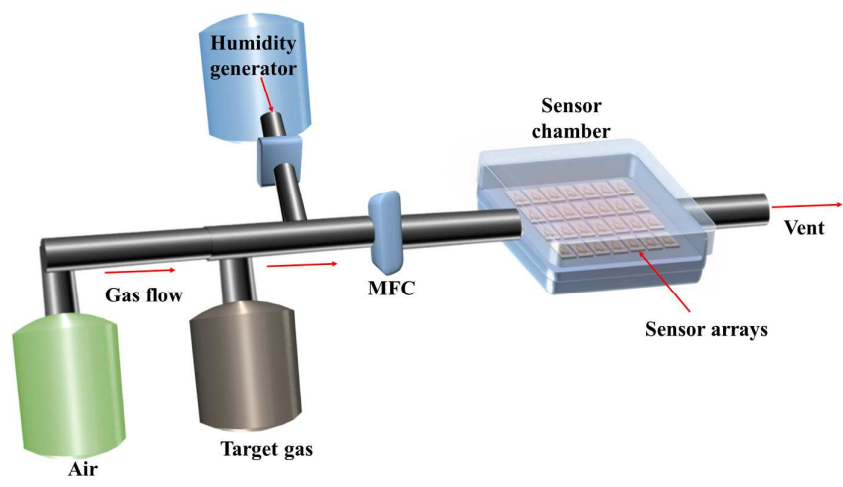


Figure S16. Schematic image of sensing measurement system.

Table S1. The pH values of 4 ZIFs solutions

Solution	pH
DI water+Co ions + HMIM	8.47
Methanol+Co ions + HMIM	7.59
DI water/EtOH (2/1) + Co ions + HMIM, belt	8.22
DI water/EtOH (1/2) + Co ions + HMIM, rod	8.05

Table S2. Grain sizes of samples based on the (100), (002), and (101) peaks.

	450 double-Co ₃ O ₄ rods@ZnO sheet	550 double-Co ₃ O ₄ rods@ZnO sheet	650 double-Co ₃ O ₄ rods@ZnO sheet	750 double-Co ₃ O ₄ rods@ZnO sheet
(100)	30.7 nm	54.6 nm	71.9 nm	92.5 nm
(002)	35 nm	55.6 nm	71.3 nm	94.4 nm
(101)	29.5 nm	50.5 nm	65.2 nm	91.2 nm
Aver.	31.7 nm	53.6 nm	69.5 nm	92.7 nm

Table S3. ICP results of single-Co₃O₄ NRs@ZnO NSs, double-Co₃O₄ NRs@ZnO NSs, and triple-Co₃O₄ NRs@ZnO NSs

ICP analysis		
Samples	Co (%)	Zn (%)
single-Co ₃ O ₄ NRs@ZnO NSs	0.27	80.0
double-Co ₃ O ₄ NRs@ZnO NSs	0.71	79.6
triple-Co ₃ O ₄ NRs@ZnO NSs	1.82	78.4

Table S4. The surface area under XPS spectra of O 1s in single-Co₃O₄ rods@ZnO sheet, double-Co₃O₄ rods@ZnO sheet, and triple-Co₃O₄ rods@ZnO sheet.

Spectral Feature Table			
Element/Transition	Peak Energy (eV)	Peak Area (eV counts)	O⁻/O²⁻
O ²⁻ (1s) in Single-Co ₃ O ₄ NRs@ZnO NSs	530.2	60693.83	0.615
O ⁻ (1s) in Single-Co ₃ O ₄ NRs@ZnO NSs	531.0	37325.69	
O ²⁻ (1s) in Double-Co ₃ O ₄ NRs@ZnO NSs	530.2	47322.30	1.203
O ⁻ (1s) in Double-Co ₃ O ₄ NRs@ZnO NSs	531.0	56943.89	
O ²⁻ (1s) in Triple-Co ₃ O ₄ NRs@ZnO NSs	530.2	54250.09	0.727
O ⁻ (1s) in Triple-Co ₃ O ₄ NRs@ZnO NSs	531.0	39428.26	

Table S5. Recent publications on MOF derived SMOs based chemiresistive acetone sensors.

Gas species	Materials	Optimal temperature	Limit of detection	Response	Reference
Acetone	ZnO@ZIF-CoZn nanowire	260 °C	1.9 ppb	12–13.5 @ 5 ppm	1
	MOF templated Cu ₂ O/CuO cages	150 °C	N/A	2.6–3 @ 200 ppm	2
	MOF templated ZnO nanocages	300 °C	100 ppb	2.2 @ 0.1 ppm	3
	MOF templated PdO-ZnO loaded SnO ₂ nanotubes	400 °C	10 ppb	10 @ 5 ppm	4
	MOF templated ZnO/ZnCo ₂ O ₄ hollow spheres	250 °C	N/A	1.7 @ 5 ppm	5
	MOF derived PdO loaded Co ₃ O ₄ cubes	350 °C	0.1 ppm	2.51 @ 5 ppm	6
	MOF templated ZnO/ZnFe ₂ O ₄ nanospheres	290 °C	1 pm	10 @ 25 ppm, 5 @ 5 ppm	7
	MOF derived Co ₃ O ₄ /NiCo ₂ O ₃ double-shelled cages	228.9 °C	N/A	3.09 @ 100 ppm	8
	MOF derived Co ₃ O ₄ -PdO loaded n-SnO ₂ HNCs	450 °C	5 ppb	22.8 @ 5ppm	9
HMOF template double-Co ₃ O ₄ rods@ZnO sheet	450 °C	5 ppb	29@5 ppm	this work	

Table S6. Recent publications on MOF based chemiresistive sensors.

Gas species	Materials	Optimal temperature	Detection limit	Response	Reference
H ₂ S	ZIF-8	Room temperature	N/A	3 @ 1ppm	10
n-butanol	SNNU-50	Room temperature	N/A	1.56 @ 100 ppm	11
H ₂ S	Cu(bdc) xH ₂ O	Room temperature	N/A	1–2 @ 1ppm	10
H ₂ S	Fumarate based fcu-MOF	Room temperature	5.4 ppb	12–15 @ 10 ppm	10, 12
N(CH ₃) ₃ (Trimethyl amine)	Co(im) ₂ MOF	75 °C	2 ppm	14 @ 100 ppm	13
MeOH Acetone	Cu ₃ (HTTP) ₂	Room temperature	N/A	1.08 @ 200 ppm (EtOH), ~1.02 @ 200 ppm (acetone)	14
EtOH Acetone	Ni ₃ (HITP) ₂	Room temperature	N/A	1.03–1.04 @ 200 ppm (EtOH), ~1.02 @ 200 ppm (acetone)	14, 15
MeOH	MIL-53-NH ₂ (Al)@polymer	Room temperature	N/A	2.49 @ 5000 ppm	16, 17
Formaldehyde Acetone	ZIF-67	150 °C	5 ppm	13 @ 100 ppm (Formaldehyde) 7 @ 100 ppm (acetone)	18
Acetone	MOF derived Co ₃ O ₄ -PdO loaded n-SnO ₂ HNCs	450 °C	5 ppb	22.8 @ 5ppm	9
Acetone	HMOF template double-Co ₃ O ₄ rods@ZnO sheet	450 °C	5 ppb	29@5 ppm	this work

References

1. Yao, M. S.; Tang, W. X.; Wang, G. E.; Nath, B.; Xu, G. MOF Thin Film Coated Metal Oxide Nanowire Array: Significantly Improved Chemiresistor Sensor Performance. *Adv. Mater.* **2016**, *28*, 5229-5234.
2. Wang, Y.; Lü, Y.; Zhan, W.; Xie, Z.; Kuang, Q.; Zheng, L. Synthesis of porous Cu₂O/CuO Cages using Cu-based Metal-organic Frameworks as Templates and Their Gas-sensing Properties. *J. Mater. Chem. A*, **2015**, *3*, 12796.
3. Li, W.; Wu, X.; Han, N.; Chen, J.; Qian, X.; Deng, Y.; Tang, W.; Chen, Y. MOF-derived Hierarchical Hollow ZnO Nanocages with Enhanced Low-concentration VOCs Gas-sensing Performance. *Sensor. Actuat. B: Chem.*, **2016**, *225*, 158.
4. Koo, W.-T.; Jang, J.-S.; Choi, S.-J.; Cho, H.-J.; Kim, I.-D. Metal-Organic Framework Templated Catalysts: Dual Sensitization of PdO-ZnO Composite on Hollow SnO₂ Nanotubes for Selective Acetone Sensors. *ACS Appl. Mater. Inter.* **2017**, *9*, 18069.
5. Koo, W.-T.; Choi, S.-J.; Jang, J.-S.; Kim, I.-D. Metal-Organic Framework Templated Synthesis of Ultrasmall Catalyst Loaded ZnO/ZnCo₂O₄ Hollow Spheres for Enhanced Gas Sensing Properties. *Sci. Rep.* **2017**, *7*, 45074.
6. Koo, W.-T.; Yu, S.; Choi, S.-J.; Jang, J.-S.; Cheong, J. Y.; Kim, I.-D. Nanoscale PdO Catalyst Functionalized Co₃O₄ Hollow Nanocages Using MOF Templates for Selective Detection of Acetone Molecules in Exhaled Breath. *ACS Appl. Mater. Inter.*, **2017**, *9*, 8201-8210.
7. Wang, X.; Zhang, S.; Shao, M.; Huang, J.; Deng, X.; Hou, P.; Xu, X. Fabrication of ZnO/ZnFe₂O₄ Hollow Nanocages Through Metal Organic Frameworks Route with Enhanced Gas Sensing Properties. *Sensor. Actuat. B: Chem.*, **2017**, *251*, 27.
8. Qu, F.; Jiang, H.; Yang, M. MOF-derived Co₃O₄/NiCoO₄ double-shelled nanocages with excellent gas sensing properties. *Mater. Lett.*, **2017**, *190*, 75.-78.
9. Jang, J.-S.; Koo, W.-T.; Choi, S.-J.; Kim, I.-D. Metal Organic Framework-Templated Chemiresistor: Sensing Type Transition from P-to-N Using Hollow Metal Oxide Polyhedron via Galvanic Replacement. *J. Am. Chem. Soc.* **2017**, *139*, 11868-11876
10. Yassine, O.; Shekhah, O.; Assen, A. H.; Belmabkhout, Y.; Salama, K. N.; Eddaoudi, M. H₂S Sensors: Fumarate-Based fcu-MOF Thin Film Grown on a Capacitive Interdigitated Electrode. *Angew. Chem. Int. Edit* **2016**, *55*, 15879-15883.
11. Bai, X.-Y.; Ji, W.-J.; Li, S.-N.; Jiang, Y.-C.; Hu, M.-C.; Zhai, Q.-G. Nonlinear Optical Rod Indium-Imidazolecarboxylate Framework as Room-Temperature Gas Sensor for

Butanol Isomers. *Cryst. Growth Des.* **2016**, *17*, 423-427.

12. Campbell, M. G.; Dincă, M. Metal–Organic Frameworks as Active Materials in Electronic Sensor Devices. *Sensors* **2017**, *17*, 1108.

13. Chen, E.-X.; Fu, H.-R.; Lin, R.; Tan, Y.-X.; Zhang, J. Highly Selective and Sensitive Trimethylamine Gas Sensor Based on Cobalt Imidazolate Framework Material. *ACS Appl. Mater. Inter* **2014**, *6*, 22871.

14. Campbell, M. G.; Liu, S. F.; Swager, T. M.; Dincă, M. Chemiresistive Sensor Arrays from Conductive 2d Metal–organic Frameworks. *J. Am. Chem. Soc.* **2015**, *137*, 13780-13783.

15. Wu, G.; Huang, J.; Zang, Y.; He, J.; Xu, G. Porous Field-effect Transistors Based on a Semiconductive Metal–organic Framework. *J. Am. Chem. Soc.* **2016**, *139*, 1360-1363.

16. Stassen, I.; Burtch, N.; Talin, A.; Falcaro, P.; Allendorf, M.; Ameloot, R. An updated roadmap for the integration of metal–organic frameworks with electronic devices and chemical sensors. *Chem. Soc. Rev.* **2017**, *46*, 3185-3241.

17. Sachdeva, S.; Socol, D.; Gravesteijn, D. J.; Kapteijn, F.; Sudhölter, E. J.; Gascon, J.; de Smet, L. C. Polymer–Metal Organic Framework Composite Films as Affinity Layer for Capacitive Sensor Devices. *ACS Sensors* **2016**, *1*, 1188-1192.

18. Chen, E.-X.; Yang, H.; Zhang, J. Zeolitic Imidazolate Framework as Formaldehyde Gas Sensor. *Inorg. Chem.* **2014**, *53*, 5411-5413.